Supporting Information

Marturano et al. 10.1073/pnas.1300135110

SI Materials and Methods

Reagents. Unless otherwise stated, all chemical reagents were purchased from Sigma–Aldrich. Dulbecco's modified PBS (DPBS; without Ca^{2+}/Mg^{2+}), HBSS, and DAPI stain were from Invitrogen.

Chick Culture and Tendon Isolation. All animal procedures received prior approval from the university institutional animal care and use committee board. Fertilized white leghorn chicken (*Gallus gallus*) eggs were obtained from the University of Connecticut poultry farm and cultured in a humidified, rocking incubator at 37.5 °C. After specified incubation times, the embryos were killed and staged according to Hamburger and Hamilton stage (HH) (1). Lower limbs were excised, and the calcaneus tendon was mechanically dissected from surrounding tissue. Because tendon tissue is not grossly visible at HH 28 or 30, the lower limbs were removed at the hip at these stages, the feet were removed, and the lower two-thirds of the remaining limb were used for analysis. This area was chosen based on preliminary data using histological staining to identify tendon, as well as reported immunohistochemical staining indicating that tenascin-positive cells are present primarily in the middle and distal regions of the lower limb at these stages (2).

β-Aminopropionitrile Treatment to Inhibit Lysyl Oxidase Activity. Chicken embryos were treated with lysyl oxidase (LOX) inhibitor β-aminopropionitrile (BAPN) *in ovo* for 24 h. At 24 h before specified stages, chicken embryos were injected *in ovo* with BAPN in saline by creating a small hole in the shell with a rotary tool and injecting 200 μL of prewarmed BAPN or saline (control) via the chorioallantoic membrane as previously described (3). The shell was then sealed with hot paraffin, and the egg was cultured at 37.5 °C for 24 h.

Because we injected BAPN into the egg of the chicken embryo, we also treated tendon explants with BAPN to investigate if systemic effects may have indirectly influenced tendon mechanical properties. However, BAPN treatment of tendon explants produced a similar reduction in elastic modulus as *in ovo* treatment (Fig. S8*A*), without affecting cell viability, proliferation, and metabolic activity (Fig. S7). Additionally, although LOX may cross-link elastin, we focused on collagen because elastin fibers were not detected embryonically in our samples with Verhoeff–Van Gieson staining (Fig. S4) or in a previous study (4).

Sample Preparation for Force Volume-Atomic Force Microscopy. For force volume (FV)-atomic force microscopy (AFM) mechanical measurements, tendons were immersed in 10% (vol/vol) DMSO in HBSS for 15 min, embedded in optimal cutting temperature (OCT) medium (Sakura Finetek USA), and slowly frozen at approximately −1 °C/min to −80 °C in an isopropanol bath. The freezing protocol was based on previous studies demonstrating that freezing arterial vessels (5–7) or type I collagen gels (8, 9) in this manner does not result in a significant change in bulk elastic modulus after thawing. In addition, we did not expect the mechanical contribution of proteoglycans to be affected by this freeze–thaw process, because the mechanical properties of adult bovine articular cartilage, a proteoglycan-rich tissue, were not significantly affected ($P > 0.05$) after freeze–thaw from −20 °C (10) or −80 °C (11). Frozen tissue blocks were then mounted in a −19 °C cryostat (CM1950; Leica Microsystems) with a −22 °C sample block temperature and sectioned longitudinally at a thickness of 20 μm. Sections were transferred onto polylysine-coated glass slides (Thermo Scientific) and immersed in DPBS for 1 min to remove OCT. Sections were then placed in a separate DPBS bath for immediate FV-AFM measurements.

For tendon explants, chicks staged at HH 40 were killed and whole lower limbs were harvested and cultured at 37 °C in complete medium consisting of DMEM and 10% (vol/vol) FBS for 24 h with or without 5 mg of BAPN per gram of dry tissue weight. Afterward, tendon tissue was extracted, embedded in OCT, and cryosectioned as described above. FV-AFM maps were captured at 16 × 16 indentation resolution over 10 × 10-μm areas.

FV-AFM and Data Collection. An atomic force microscope (Dimension 3100 with a low noise scanner; Bruker) with a commercial fluid cell was used. For nanoscale tip measurements, an Si_3N_4 probe with an ∼20-nm tip radius and a spring constant of 0.06 N/m (Bruker) was used. For microscale tip measurements, a 5-μm radius SiO_2 sphere (Corpuscular) was attached with epoxy to tipless probes with a 0.06-N/m spring constant (Bruker). Cantilever deflection was calibrated before each measurement using mica disks (Ted Pella) in DPBS. The FV mode was used to capture indentation force curves at nodes of a 2D array. Maps with nanoscale tips were recorded over a 10 × 10-μm tissue area in a 64 × 64 array of force curves, with 128 sampling points each. For microscale tips, single indentation force curves were recorded over 40 × 40-μm tissue areas in a 2 × 2 array, also with 128 sampling points each. The probes were descended until a 40-nm cantilever deflection or a 1.0- or 1.2-μm indentation travel was reached for micro- and nanotips, respectively. The limitation on total indentation depth was chosen to minimize contributions from the underlying substrate by indenting a maximum of 6% of the tissue thickness (12).

To maintain tissue hydration, FV-AFM measurements were captured with tissue submerged in DPBS. All measurements were performed at room temperature (22–24 °C). The area to be measured via FV-AFM in a section was carefully selected using a dissecting microscope and locating a tissue area with the fibrous morphology of tendon midsubstance. Probes were engaged with a 6-μm/s indentation rate, previously shown to measure elastic properties of hydrogels using microscale tips (13). Additionally, we have analyzed the effects of varying indentation rates between 0.1 and 18 μm/s on indentation slopes for agarose gels and between HH 28 (early-stage) and HH 43 (late-stage) chick tendon. Despite varying the indentation slope by nearly two orders of magnitude around the rate used, we found no indentation rate dependence on indentation slope for any of the samples (Fig. S9*A*). We therefore concluded that an indentation rate of 6 μm/s principally measures elastic properties and that viscous contributions are negligible at this rate.

Calculation of Elastic Modulus. The slopes of the linear regions of extension curves were calculated using least-square linear regression with a custom Visual Basic module (Microsoft Corporation). Indentation slope was converted to elastic modulus with two methods: (*i*) empirically based on agarose gel standards (14) or (*ii*) theoretically based on Hertzian indentation mechanics.

Agarose gels were prepared by mixing agarose (molecular biology grade; Fisher Scientific) with dH_2O and heating to 90 °C. These solutions were cast into 35-mm-diameter dishes, and indentation slopes were captured in DPBS from three cantilevers each for nano- and microscale tips. Macroscale compression testing was used to quantify compressive elastic modulus of agarose gels tested with AFM. Gel cylinders with a 1:1 height-to-diameter ratio (15) were extracted with a biopsy punch to

minimize meniscus effects. Compression was applied with an electromechanical crosshead system (Instron 3360) and a 10-N load cell. The platens were thinly coated with silicone oil to minimize friction, and samples were subjected to unconfined uniaxial compression to 10% strain at 0.1% strain per second, and the linear region ($r^2 \geq 0.995$) of the stress-strain curve was taken as the elastic modulus. Elastic moduli were plotted against the indentation slope to derive a standard curve (Fig. S1).

Elastic moduli based on Hertzian indentation mechanics were calculated for nano- and microscale measurements. For nanoscale-diameter probes, we used the pyramidal tip indentation model developed by Loparic et al. (16):

$$E_{nano} = \frac{(1-\nu^2)S}{2h \cdot \tan\theta}, \quad \textbf{[S1]}$$

where E_{nano} is elastic modulus calculated for nanoscale tips, ν is Poisson's ratio, S is the slope of the linear region of the force-displacement curve, h is the depth of indentation, and θ is the half-opening angle of the pyramidal tip. We estimated h by extrapolating the linear region of each force curve to zero force and compensating for cantilever deflection. We assumed volume conservation with $\nu = 0.5$ and used a value for θ provided by the manufacturer (Bruker). For microscale-diameter probes, a spherical tip indentation model was used (17):

$$E_{micro} = \frac{\sqrt{\pi}}{2}(1-\nu^2)\frac{S}{\sqrt{A}}, \quad \textbf{[S2]}$$

where E_{micro} is elastic modulus calculated for microscale tips and A is the projected contact area of the spherical indenter at full indentation depth. The contact area A was estimated using the method of Loparic et al. (16):

$$A = \pi \cdot (h(2r-h)), \quad \textbf{[S3]}$$

where r is the radius of the indenter.

In our analyses, we calculated sample elastic modulus from AFM measurements using both empirical and theoretical methods. Hertzian indentation theory requires knowledge of the initial tip-sample contact point (17), which is difficult to determine for biological samples due to rough surface topography, electrostatic interactions, and adhesion effects (14, 18). On the other hand, empirical analysis methods typically use compression testing to measure modulus of the standard material (14), whereas AFM uses indentation testing. We found that the magnitudes and trends of moduli with time are in close agreement between both methods of analysis.

DNA and Cellularity Quantification. Tendon samples were blotted to remove excess saline and were weighed before and after lyophilization for 96 h. The DNA-to-dry mass ratio was quantified with UV absorbance after DNA purification (19). Lyophilized tissue was digested overnight with 10 mg/mL sodium dodecyl sulfate (SDS) and 200 μg/mL proteinase K at 60 °C and 0.88 × *g*. Next, DNA was isolated using 25:24:1 phenol/chloroform/isoamyl alcohol and precipitated with 115 mM sodium acetate in −20 °C ethanol. DNA was then pelleted at 12,000 × *g* for 15 min, washed with 70% (vol/vol) ethanol, and resuspended in 10 mM Tris (hydroxymethyl) aminomethane (Tris) and 1 mM EDTA (TE) buffer. DNA concentration was measured at 260-nm absorbance (BioPhotometer plus; Eppendorf) against a TE blank, and DNA mass was calculated by multiplying concentration by suspension volume. Cellularity, defined as nuclei per square area, was measured by staining 8-μm paraffin sections of HH 43 tendon tissue and counting nuclei in tendon fascicles from H&E-stained sections over 100 × 100-μm areas. Nuclei from at least eight sections were counted per chick tendon.

Glycosaminoglycan Quantification. Tendon samples were lyophilized for 96 h and digested in 200 μg/mL proteinase K overnight at 60 °C and 0.88 × *g* in preparation for glycosaminoglycan (GAG) quantification. Total sulfated GAG mass was measured with a precipitation-based 1,9-dimethymethylene blue chloride (DMMB; Polysciences) assay (20). A 100-μL aliquot of standard or digested tendon was added to 1 mL of DMMB working dye solution [16 μg/mL DMMB, 0.2 M guanidine hydrochloride, 5% (vol/vol) ethanol, 0.2% (vol/vol) formic acid, 0.2% (wt/vol) sodium formate] and mixed at room temperature for 30 min. The DMMB–GAG complex was pelleted at 12,000 × *g* for 10 min, and the supernatant was discarded. Afterward, 1,100 μL of dissociation reagent [4 M guanidine hydrochloride, 10% (vol/vol) *n*-propanol, 0.41% (wt/vol) sodium acetate] was added to solubilize the DMMB molecules. The absorbance at 656 nm of the resulting solution was measured (SpectraMax M2; Molecular Devices) in triplicate against a dissociation reagent blank. Chondroitin sulfate (CS) was used as a standard (Fig. S9*B*).

We found that chick DNA binds to DMMB with similar affinity as CS either in isolation or in spiked tissue digests (Fig. S9 *C* and *D*), despite DNase or microfiltration treatment (Fig. S9 *E* and *F*). Therefore, we subtracted DNA mass from the raw GAG absorbance value. For GAG-to-dry mass ratios, we used:

$$\text{GAG/dry mass} = \frac{m_{GAGraw} - m_{DNApk}}{m_{dry}}, \quad \textbf{[S4]}$$

where m_{GAGraw} is the total GAG mass from the raw absorbance reading, m_{DNApk} is the total DNA mass isolated from proteinase K digests, and m_{dry} is the total dry mass. For GAG-to-DNA mass ratios, we used:

$$\text{GAG/DNA mass} = \frac{m_{GAGraw} - m_{DNApk}}{m_{DNApk+sds}}, \quad \textbf{[S5]}$$

where $m_{DNApk+sds}$ is the total DNA mass after a second overnight digestion with 200 μg/mL proteinase K and 10 mg/mL SDS in TE buffer at 60 °C and 0.88 × *g*. This was done to mimic the conditions used for DNA isolation for DNA-to-dry mass ratio quantification. SDS was not included in the original digest due to its strong affinity to DMMB (21).

Hydroxyproline Quantification. Hydroxyproline (Hyp) mass was quantified using a *p*-dimethylaminobenzaldehyde (DMAB) absorbance method (22). Tendon was dissected, washed with dH_2O, and lyophilized for 96 h to obtain dry mass. HCl was added to produce a 5-mg/mL concentration of dry tissue mass in 6 N of HCl. Tendons were then hydrolyzed at 110 °C for 24 h. Afterward, the tubes were evaporated and dry mass was resuspended in dH_2O at a concentration of 10 mg/mL. Up to 50 μL of this digest was added to 250 μL of chloramine T reagent at pH 6.5 [12.7 mg/mL chloramine T in 2 mL of 50% (vol/vol) *n*-propanol, adjusted to 10 mL with 0.88 M sodium acetate, 0.85 M potassium hydroxide, 4.6% (wt/vol) citric acid, 1.2% (vol/vol) acetic acid] and allowed to oxidize at room temperature for 25 min. Afterward, 300 μL of Ehrlich's reagent [1 M DMAB in 66% (vol/vol) *n*-propanol, 33% (vol/vol) perchloric acid] was added and the chromophore was developed at 65 °C for 20 min. From this, absorbance was measured in triplicate at 550 nm. A standard using trans-4-hydroxy-L-proline was used to quantify Hyp content from absorbance readings (SpectraMax M2; Molecular Devices) (Fig. S9*G*).

Histological Analysis. Histological staining was performed on tendons using paraffin embedding and microtome sectioning.

Tendons were excised, fixed in 10% (vol/vol) formalin (pH 7.4), embedded in paraffin, and sectioned at a thickness of 8 μm. Consecutive sections were then deparaffinized with xylene and stained in either 0.1% wt/vol Sirius red (C.I. 35780; Polysciences) in saturated picric acid for 60 min (23), 1% wt/vol Alcian blue 8GX (C.I. 74240; Polysciences) adjusted to pH 2.5 with acetic acid for 30 min (24), or solutions of hematoxylin (Gill no. 2) for 10 min and eosin (Y alcoholic) for 10 s. Sections were dehydrated, cleared, and mounted in dibutyl phathalate xylene mountant. Images of tendon midsubstance were captured on an inverted optical microscope (Diavert; Leitz Wetzlar) with a color camera (ExwaveHAD; Sony) and 97× oil immersion objective (N.A. = 1.3).

To determine if observed GAG deposits were cell nuclei, serial staining was also performed on 8-μm sections, using either staining with Alcian blue followed by DAPI (Fig. 2*D*; 500 ng/mL in DPBS) or staining with DAPI followed by Alcian blue (Fig. S3*A*). Brightfield and fluorescence images (excitation 360 ± 20 nm/emission 470 ± 20 nm) were captured at eight-bit grayscale resolution on an inverted optical microscope (DMIL; Leica) with a monochrome camera (DFC365 FX; Leica) using a 40× air objective. Brightfield pixel intensities were inverted, such that pixels of high light absorbance corresponded to high pixel intensities. For spatial determination of overlap, inverted brightfield images were set to the red channel and represented Alcian blue staining, and DAPI fluorescence was set to the green channel. Colocalized pixels were set to yellow, and overlays were generated using ImageJ version 1.44j (National Institutes of Health).

Multiphoton Microscopy for Collagen Structure. To examine changes in collagen structure during development, multiphoton microscopy was used. Fresh, unfixed tendon tissue from HH 28–43 chicks was cryosectioned at a thickness of 20 μm and coverslipped in saline. Second harmonic generation (SHG) images were captured on a laser scanning confocal microscope (TCS SP2; Leica) with 800-nm incident light from a tunable Ti:sapphire laser (Mai Tai; Spectra Physics). Forward SHG was detected through a 400 ± 10-nm bandpass filter designed for two-photon imaging (HQ400/20 m-2P; Chroma). For examination of changes to collagen structure during development, a 63× water immersion objective was used (N.A. = 1.2), and constant dwell time and photomultiplier tube gain were used for all images. Only a 10 × 10-μm field, coinciding with the FV-AFM field, was sampled by 512 × 512 pixels.

To examine changes in collagen structure after BAPN treatment, SHG images were captured as described above with minor differences. Whole, fresh tendon sections ∼1 mm in thickness were placed into glass-bottom dishes (14-mm glass well; In Vitro Scientific), immersed in saline, and imaged using forward SHG as described above at either low or high zoom settings, providing 512 × 512-pixel frames of either a 238 × 238-μm or 40 × 40-μm field, respectively. The incident power and detector settings were the same for all samples of a given developmental stage.

Overlay and Imaging Correlation of Elastic Modulus with Multiphoton Confocal Microscopy. Overlays of FV-AFM elastic modulus maps and multiphoton microscopy of the tissue surface were captured on fresh tendon cryosections, which were maintained hydrated during all steps. First, longitudinal cryosections (20-μm thickness) of unfixed, fresh HH 43 tendon were marked with fresh Verhoeff staining solution using glass micropipettes under a magnification of 10×. Verhoeff stain was applied to areas of tendon midsubstance in patterns resembling the vertices of a triangle ∼200 μm apart. These small (∼50-μm diameter) markers facilitated colocalization of AFM and confocal microscopy images. After marking, FV-AFM elastic modulus maps were then captured using 64 × 64 indentation resolution over 10 × 10-μm areas as previously described. However, the area probed relative to the Verhoeff markers was captured photographically using the built-in AFM light microscope camera (Fig. 1*A*). Afterward, cryosections were fixed in 10% (vol/vol) formalin (pH 7.4) for 20 min at room temperature and then sequentially stained in DAPI solution followed by Alcian blue as previously described.

Immediately following staining, sections were imaged on the previously described laser scanning confocal microscope (TCS SP2) after coverslipping with saline. A 63× water immersion lens (N.A. = 1.2) and a scanning resolution of 17.2 pixels per micrometer were used for all overlay imaging on the confocal microscope. First, an inverted transmittance image (i.e., an absorbance image) was captured at A_{488} while focusing on the tissue surface (Fig. 1*A*). This image provided contrast between the tissue surface and the Verhoeff staining markers, the latter of which heavily absorbed the light. Next, an image at A_{633} of the surface was captured on the same area to represent Alcian blue staining due to the high absorbance of the dye at this wavelength (25). This image showed locations of GAG deposits (Figs. 2*E* and 3*A*). Multiphoton microscopy was then used to image surface collagen fibers and cell nuclei considered to be at or within a few microns of the tissue surface due to the precision excitation volume of multiphoton microscopy (26). To avoid excess heating of the tissue, the multiphoton laser was focused on a smaller area between the Verhoeff markers to avoid direct irradiation of Verhoeff stain (Fig. 1*A*). For imaging of cell nuclei, DAPI was excited using two-photon excitation with a Ti:sapphire laser (ex. 750 nm, em. 445 ± 25 nm) at 10 mW of sample incident power. For imaging of collagen fibers, forward SHG was captured as previously described, at 20 mW of sample incident power.

After imaging, overlays were produced by aligning the Verhoeff markers from the AFM microscope image to the A_{488} image and other confocal images using transparency functions in image analysis software. The area probed by FV-AFM on confocal images was resolved by accounting for the distance of the probe tip from the end of the cantilever as supplied by the manufacturer (Bruker).

Statistical Analysis. For all statistical comparisons, type I error was set to 0.05 ($\alpha = 0.05$) unless otherwise specified; P values below 0.05 were considered to be "significant." In this study, all statistical comparisons were between three or more groups. Hence, a one-way ANOVA was used for all tests, with either a Dunnett's or Tukey's posttest depending on whether the comparison was against a control group or not, respectively. Data are reported as the mean ± SD. All calculations were performed with Prism version 5 (GraphPad).

1. Hamburger V, Hamilton HL (1951) A series of normal stages in the development of the chick embryo. *J Morphol* 88(1):49–92.
2. Kardon G (1998) Muscle and tendon morphogenesis in the avian hind limb. *Development* 125(20):4019–4032.
3. Levene CI, Gross J (1959) Alterations in state of molecular aggregation of collagen induced in chick embryos by beta-aminopropionitrile (lathyrus factor). *J Exp Med* 110:771–790.
4. Brown JP, Lind RM, Burzesi AF, Kuo CK (2012) Elastogenic protein expression of a highly elastic murine spinal ligament: The ligamentum flavum. *PLoS ONE* 7(6):e38475.
5. Adham M, et al. (1996) Mechanical characteristics of fresh and frozen human descending thoracic aorta. *J Surg Res* 64(1):32–34.
6. Blondel WCPM, Lehalle B, Maurice G, Wang X, Stoltz JF (2000) Rheological properties of fresh and cryopreserved human arteries tested in vitro. *Rheol Acta* 39(5):461–468.
7. Venkatasubramanian RT, Grassl ED, Barocas VH, Lafontaine D, Bischof JC (2006) Effects of freezing and cryopreservation on the mechanical properties of arteries. *Ann Biomed Eng* 34(5):823–832.
8. Devireddy RV, Neidert MR, Bischof JC, Tranquillo RT (2003) Cryopreservation of collagen-based tissue equivalents. I. Effect of freezing in the absence of cryoprotective agents. *Tissue Eng* 9(6):1089–1100.
9. Neidert MR, Devireddy RV, Tranquillo RT, Bischof JC (2004) Cryopreservation of collagen-based tissue equivalents. II. Improved freezing in the presence of cryoprotective agents. *Tissue Eng* 10(1-2):23–32.
10. Changoor A, Fereydoonzad L, Yaroshinsky A, Buschmann MD (2010) Effects of refrigeration and freezing on the electromechanical and biomechanical properties of articular cartilage. *J Biomech Eng* 132(6):064502.

11. Szarko M, Muldrew K, Bertram JE (2010) Freeze-thaw treatment effects on the dynamic mechanical properties of articular cartilage. *BMC Musculoskelet Disord* 11:231.
12. Persch G, Born C, Utesch B (1994) Nano-hardness investigations of thin-films by an atomic-force microscope. *Microelectron Eng* 24(1-4):113–121.
13. Mahaffy RE, Shih CK, MacKintosh FC, Käs J (2000) Scanning probe-based frequency-dependent microrheology of polymer gels and biological cells. *Phys Rev Lett* 85(4): 880–883.
14. Stolz M, et al. (2004) Dynamic elastic modulus of porcine articular cartilage determined at two different levels of tissue organization by indentation-type atomic force microscopy. *Biophys J* 86(5):3269–3283.
15. Normand V, Lootens DL, Amici E, Plucknett KP, Aymard P (2000) New insight into agarose gel mechanical properties. *Biomacromolecules* 1(4):730–738.
16. Loparic M, et al. (2010) Micro- and nanomechanical analysis of articular cartilage by indentation-type atomic force microscopy: Validation with a gel-microfiber composite. *Biophys J* 98(11):2731–2740.
17. Oliver WC, Pharr GM (1992) An improved technique for determining hardness and elastic-modulus using load and displacement sensing indentation experiments. *J Mater Res* 7(6):1564–1583.
18. Candiello J, et al. (2007) Biomechanical properties of native basement membranes. *FEBS J* 274(11):2897–2908.
19. Chomczynski P, Sacchi N (2006) The single-step method of RNA isolation by acid guanidinium thiocyanate-phenol-chloroform extraction: Twenty-something years on. *Nat Protoc* 1(2):581–585.
20. Barbosa I, et al. (2003) Improved and simple micro assay for sulfated glycosaminoglycans quantification in biological extracts and its use in skin and muscle tissue studies. *Glycobiology* 13(9):647–653.
21. Müller G, Hanschke M (1996) Quantitative and qualitative analyses of proteoglycans in cartilage extracts by precipitation with 1,9-dimethylmethylene blue. *Connect Tissue Res* 33(4):243–248.
22. Reddy GK, Enwemeka CS (1996) A simplified method for the analysis of hydroxyproline in biological tissues. *Clin Biochem* 29(3):225–229.
23. Junqueira LCU, Bignolas G, Brentani RR (1979) Picrosirius staining plus polarization microscopy, a specific method for collagen detection in tissue sections. *Histochem J* 11(4):447–455.
24. Quintarelli G, Scott JE, Dellovo MC (1964) The chemical and histochemical properties of Alcian Blue. II. Dye binding of tissue polyanions. *Histochemie* 4(2):86–98.
25. Björnsson S (1993) Simultaneous preparation and quantitation of proteoglycans by precipitation with alcian blue. *Anal Biochem* 210(2):282–291.
26. Zipfel WR, Williams RM, Webb WW (2003) Nonlinear magic: multiphoton microscopy in the biosciences. *Nat Biotechnol* 21(11):1369–1377.

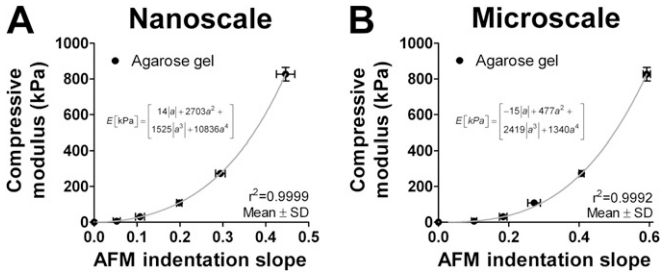

Fig. S1. Relationship between AFM indentation slope and bulk compressive modulus of agarose gels. Elastic modulus values were calculated from slopes of stress-strain curves using quasistatic compression to 10% strain as described in *SI Materials and Methods*. AFM indentation slopes measured using either nanoscale (*A*) or microscale (*B*) tips were plotted against measured compressive elastic moduli. The data were fit to fourth-order polynomial functions (shown) that were constrained through the origin. These fits were used to calculate elastic modulus from FV-AFM measurements empirically.

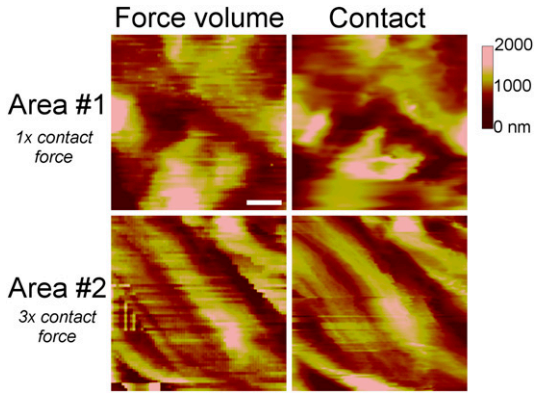

Fig. S2. FV-AFM and contact mode AFM topography scans of embryonic tendon. Two different regions (areas #1 and #2) of HH 41 embryonic chick tendon in DPBS were measured first by FV-AFM and subsequently by contact mode AFM to obtain topography scans. With either onefold (2.4 nN) or threefold (7.2 nN) contact mode force, topography is similar between the two modes. (Scale bar, 2 μm.)

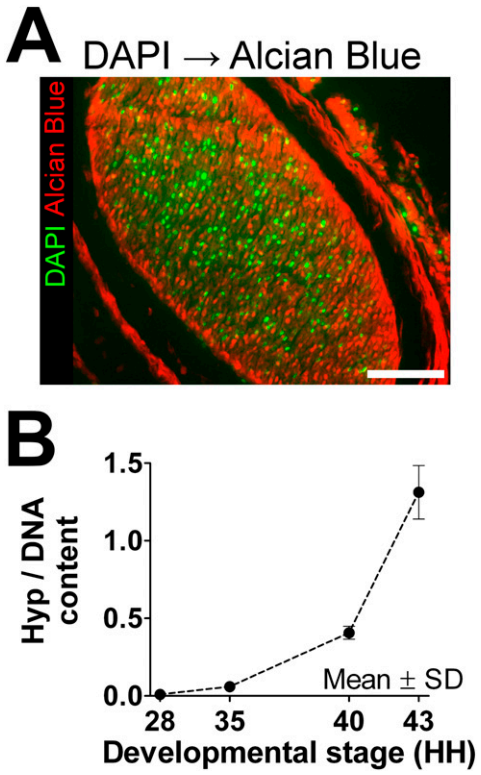

Fig. S3. (*A*) Transverse section of HH 43 embryonic tendon costained with Alcian blue and DAPI. The tendon section was first stained with Alcian blue (red channel), followed by DAPI (green channel), and then compared with Fig. 2*D*, in which DAPI staining was followed by Alcian blue staining. Staining order does not affect the appearance of distinct nuclei and GAG deposits in embryonic chick tendon, as seen in Fig. 2*D* and the current image. (Scale bar, 50 μm.) (*B*) Hyp-to-DNA content in embryonic tendon increases rapidly as a function of developmental stage.

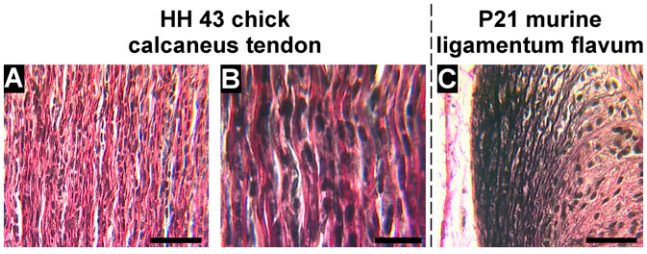

Fig. S4. Verhoeff–Van Gieson staining of HH 43 chick tendon at low (*A*) and high (*B*) magnification. (Scale bars: *A*, 50 μm; *B*, 20 μm.) Collagen fibers stained pink, and cell nuclei and elastin fibers stained black. No elastin fibers were detected at either magnification. (*C*) In contrast, elastin fibers were clearly detected in the postnatal day 21 (P21) murine ligamentum flavum, which is known to contain elastin fibers (4). (Scale bar, 50 μm.)

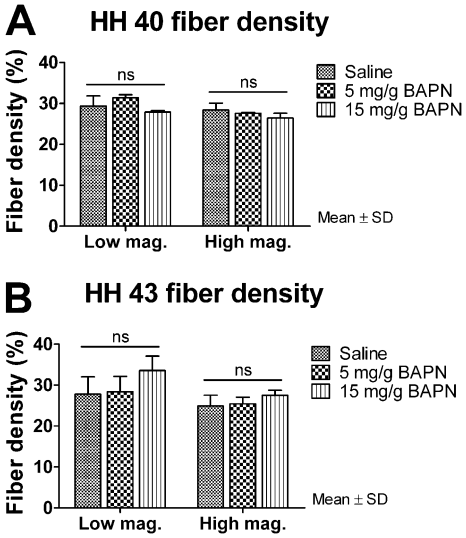

Fig. S5. BAPN treatment does not affect collagen fiber density at HH 40 (*A*) or HH 43 (*B*). Collagen fiber density of SHG images at either low-magnification ("Low mag." at 238 × 238 μm) or high-magnification ("High mag." at 40 × 40 μm) areas with a 63× objective was quantified using a published MATLAB (MathWorks) routine (1) utilizing adaptive thresholding. The results showed no statistically significant differences ($P \geq 0.16$) between saline- and BAPN-treated groups for either developmental stage or magnification. ns, not significant.

1. Bayan C, Levitt JM, Miller E, Kaplan D, Georgakoudi I (2009) Fully automated, quantitative, noninvasive assessment of collagen fiber content and organization in thick collagen gels. *J Appl Phys* 105(10):102042.

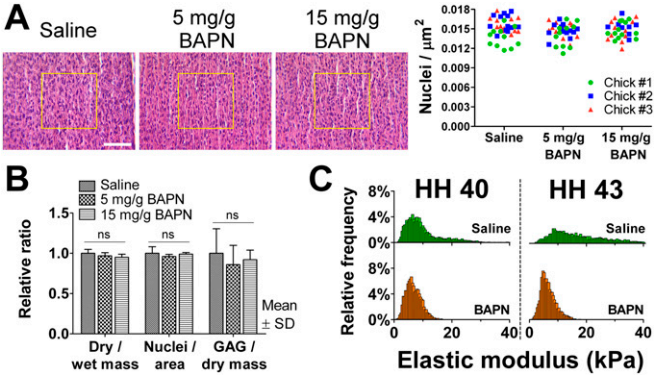

Fig. S6. (*A*) Cellular density in HH 43 tendon midsubstance as a function of BAPN dose. Histology of tendon midsubstance paraffin sections (magnification of 40×) stained with H&E. Yellow boxes represent 100 × 100-μm areas wherein nuclei were counted. (Scale bar, 50 μm.) The plot represents quantification of nuclei per square micrometer in tendon midsubstance from H&E-stained sections. Each data point represents a count from a new section, with spacing of 40 μm between sections. Average counts were not significantly different between BAPN doses ($P = 0.64$). (*B*) Effect of BAPN treatment on HH 43 embryonic tendon composition. Chicken embryos were injected *in ovo* with either saline (control) or BAPN in saline and incubated for 24 h as described earlier. Calcaneus tendons were then harvested for analysis. No statistically significant differences were found in tendon dry-to-wet mass ratio, cellularity (nuclei per area in H&E sections), or GAG-to-dry mass ratio ($P \geq 0.41$) between groups. ns, not significant. (*C*) FV-AFM elastic modulus histograms at HH 40 and 43 show a shift in distribution of modulus due to BAPN treatment, which resulted in values primarily below 15 kPa.

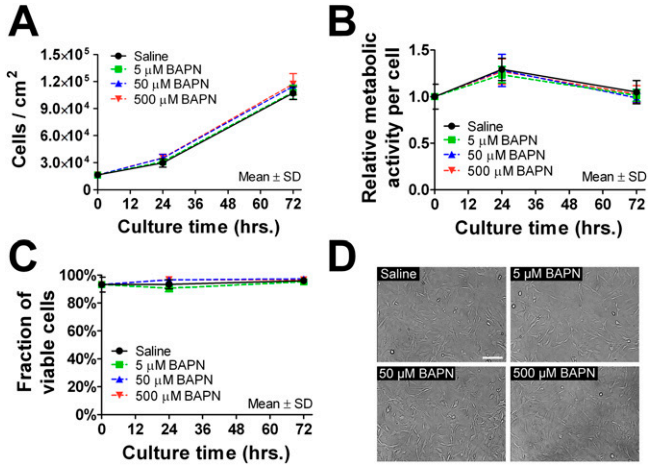

Fig. S7. Effect of BAPN treatment on embryonic tendon cell behavior in vitro. HH 42 embryonic tendon cells isolated from calcaneal tendons were cultured on tissue culture plastic and treated at 70% confluency with BAPN via medium supplementation ($t = 0$ h). BAPN concentrations were based on levels previously shown to inhibit LOX activity in vitro (1). (*A*) Cell number increased during the culture period and was not significantly affected by BAPN concentration ($P = 0.40$). (*B*) Metabolic activity per cell remained relatively constant during the culture period and was not significantly affected by BAPN dose ($P = 0.84$). (*C*) Viability remained ~95% during the culture period and was not significantly affected by BAPN dose ($P = 0.49$). (*D*) Brightfield imaging of HH 42 embryonic tendon cells after 24 h treatment with BAPN appeared fibroblastic in all groups. (Scale bar, 200 μm.)

1. Tang SS, Trackman PC, Kagan HM (1983) Reaction of aortic lysyl oxidase with beta-aminopropionitrile. *J Biol Chem* 258(7):4331–4338.

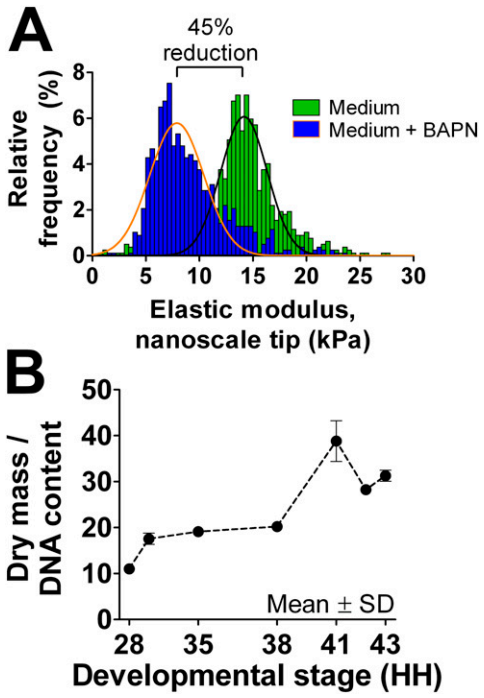

Fig. S8. (*A*) Effect of BAPN treatment on elastic modulus of HH 40 tendon explant tissue. A 45% reduction in average modulus measured with a nanoscale tip was found for BAPN-treated explant tendon compared with control tissue (no BAPN). (*B*) Tendon dry weight-to-DNA content increased progressively from HH 28–43 during development.

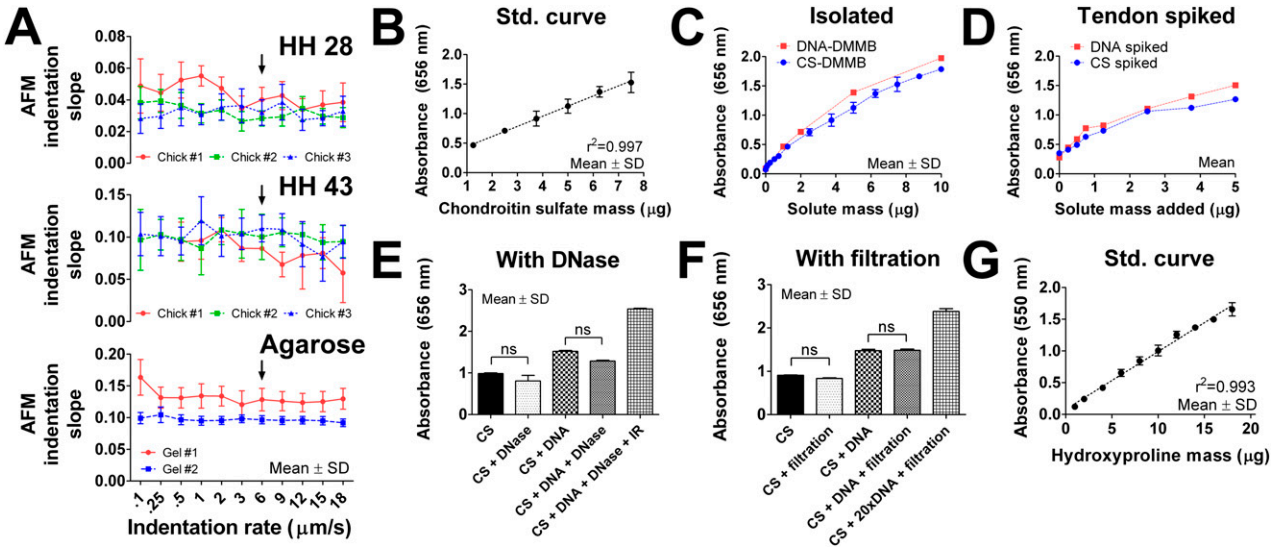

Fig. S9. (*A*) Relationship between AFM indentation rate and AFM indentation slope for HH 28 and 43 tendon and 1% agarose gels tested with nanoscale AFM tips. Black arrows indicate the AFM indentation rate used in this study. The AFM slope did not appear to be related to the indentation rate with any of the samples tested. (*B*) Development of GAG quantification method using CS standard. A standard curve of A_{656} and a CS mass between 1.25 and 7.5 μg of CS (r^2 = 0.997) were detected. (*C*) Binding affinity of isolated HH 43 chick DNA to DMMB is similar to CS. (*D*) HH 42 chick tendon digest spiked with either isolated chick DNA or CS shows similar increases in A_{656}, demonstrating that DNA content contributes substantially to GAG absorbance measurements even in tissue digests. (*E*) Influence of DNA content on A_{656} cannot be abrogated with DNase treatment. In this plot, equal amounts of GAG and DNA were added (3 μg) in the groups specified. When 5 units of TURBO DNase (Applied Biosystems) was added following the manufacturer's instructions, only 40% of the increase in A_{656} due to DNA was eliminated. Use of TURBO DNase was further confounded by the high affinity of the inactivation reagent (IR) to DMMB. (*F*) Increase in A_{656} due to DNA cannot be abrogated by microfiltration (0.22-μm filter). (*G*) Standard (Std.) curve used in quantification of hydroxyproline with absorbance assay using trans-4-hydroxy-l-proline. Plot is a linear fit between 1 and 18 μg of trans-4-hydroxy-l-proline (r^2 = 0.993).